Contents lists available at ScienceDirect

Composites Part A

journal homepage: www.elsevier.com

Mechanical properties and strain monitoring of glass-epoxy composites with graphene-coated fibers

Haroon Mahmood[a], Lia Vanzetti[b], Massimo Bersani[b], Alessandro Pegoretti[a,*]

[a] Department of Industrial Engineering, University of Trento, via Sommarive 9, 38123 Trento, Italy
[b] Centre for Materials and Microsystems, Fondazione Bruno Kessler, via Sommarive 18, 38123 Trento, Italy

ARTICLE INFO

Article history:
Received 9 August 2017
Received in revised form 5 December 2017
Accepted 21 December 2017
Available online xxx

Keywords:
A. Glass fibres
B. Fibre/matrix bond
B. Fragmentation
B. Mechanical properties

ABSTRACT

An engineered interphase can improve the mechanical properties of epoxy/glass composites simultaneously inducing a piezoresistive response. To prove this concept, E-glass fibers were coated with graphene oxide (GO) by electrophoretic deposition, while reduced graphene oxide (rGO) coated fibers were obtained by subsequent chemical reduction. The fiber-matrix interfacial shear strength measured by the single-fiber fragmentation test increased for both GO and rGO coated fibers. Unidirectional composites with a high content of both uncoated and coated fibers were produced and mechanically tested under various configurations (three-point bending, short beam shear and mode-I fracture toughness, creep). Composites with coated fibers performed similarly or better than composites prepared with uncoated fibers. Finally, composites with rGO coated fibers were tested for their piezoresistive response under both static and dynamic conditions. The electrical resistance changed proportionally to applied strain thus confirming the possibility of using composites with rGO coated fibers as strain sensors in load-bearing components.

1. Introduction

The use of polymer composites for structural and non-structural applications is rapidly expanding mainly due to their high strength-to-weight ratio and corrosion resistance. The utmost requirement in a structural composite is an high level of mechanical properties which in turn largely depends on the fiber/matrix interfacial adhesion [1]. This dependence comes from the fact that an effective load transfer from matrix to the fibers is required to exploit the superior elastic and ultimate mechanical properties of high-performance fibers. This could be assured by mechanisms such as mechanical interlocking, chemical bonding or physical adhesion at the fiber/matrix interface [2]. The poor wettability of matrix or the absence of functional groups on fiber may result in an unsatisfactory load transfer process. Both academia and industry are constantly investigating new ways to design better fiber/matrix interphases in structural composites in order to assure an optimal load transfer and possibly adding new functionalities [3].

The use of nanomaterials in polymer composites and the novel properties offered by such nanocomposites have been widely investigated in recent years. The presence of nanomaterials like clays, carbon nanotubes and graphene have been proven to largely affect the properties of both thermoplastic and thermosetting matrices [4]. Especially, the advantage of using carbonaceous nanomaterials as functional filler in polymer composites has been vastly proven due to their elevated mechanical properties and high electrical conductivity [5]. This last feature led to the possibility of self-sensing or in-situ structural health monitoring of carbon nanomaterial reinforced polymer composites like in case of CNT [6–8] and graphene [9,10]. Graphene, since its discovery in 2004, has been investigated at an exponential level in recent years due to its exceptional mechanical, electrical, optical and thermal properties [11–14]. The use of graphene in polymer composites has shown to play remarkable synergistic effects for multiple applications [15]. However, in order to obtain maximum benefit from the nanoparticles, it is necessary to reach an optimal dispersion in polymer matrices which is often quite difficult due to high surface energy of nanoparticles which results in their agglomeration [16,17].

In case of fiber reinforced polymer composites, various studies have been conducted to prove the impact of nanoparticles in enhancing various mechanical properties [18–21]. In most of the research work reported in the open scientific literature, nanoparticles were more or less homogeneously dispersed in polymer matrices in various concentrations. Another possible approach consists in depositing nanofillers on the fiber surface thus allowing a selective modification of the interphase [3]. Coating the fibers with graphene oxide nanosheets to create an interphase in polymer matrix has been recently proven to be a successful approach to enhance the load transfer at the fiber matrix interface [22,23]. Graphene coated fibers have been recently utilized for strain monitoring applications in which the coating of graphene was performed by soaking (in GO solution) [24] or dip coating process (in GNP solution) [25]. However, the use of a controlled electrophoretic deposition process to create a fairly uniform and continuous graphene coating on fibers has not yet been utilized.

* Corresponding author.
Email address: alessandro.pegoretti@unitn.it (A. Pegoretti)

https://doi.org/10.1016/j.compositesa.2017.12.023
1359-835/

Hence in this paper, we explore the creation of an interphase of GO and rGO by electrophoretic deposition on glass fibers (GF) and their usage to produce fiber reinforced polymer composites with an epoxy matrix. The interfacial properties of single fiber composites with both interphases are presented and compared in this paper along with mechanical properties of high fiber volume fraction composites. For conductive composites with rGO coated fibers, the strain-monitoring/self-sensing behavior of glass fiber/epoxy composites was also investigated in detail where the change of absolute resistance due to change in strain in composites was also monitored and analyzed.

2. Experimental

2.1. Materials

All chemicals were of analytical grade and used without additional purification. Graphite powder, potassium permanganate, sulfuric acid, sodium nitrate and hydrogen peroxide were purchased from Sigma Aldrich while hydrochloric acid was from Codec Chemical Co. Ltd. E-glass fibers (manufactured by PPG Industries, trade name XG 2089) with a diameter of 16.0 ± 0.1 μm and an epoxy-compatible sizing were used as received. A bicomponent epoxy resin (epoxy base EC 252 and hardener W 241) was provided by Elantas Europe S.r.l. (Parma, Italy). The physical properties of epoxy resin cured at room temperature for 3 h followed by 15 h at 60 °C are summarized in Table 1.

2.2. Preparation of graphene oxide and coating of glass fibers

Graphene oxide (GO) was synthesized using an approach derived from the Hummer's method [26] and described in [23]. The obtained brown solution was dried in a vacuum oven at 50 °C for at least 36 h to obtain GO powder.

A schematic description of the electrophoretic deposition (EPD) process used to deposit GO nanosheets on glass fibers (GFs) is depicted in Fig. 1. Initially, GO powder was dispersed in water (1 mg/ml) and the solution was subjected to bath-sonication for 1 h. Since GFs are non-conductive, two copper plates were used as electrodes in the EPD process. Strands of GFs (fixed on a metallic window frame) were placed near the anode since GO display negative potential due to functionalities attached during the oxidation reaction. Hence, during the EPD process graphene oxide migrated towards the anode and deposited on the GFs. EPD was carried out under an applied voltage of 10 V/cm with a constant deposition time of 5 min and a gap between the electrodes of 2 cm. A second EPD cycle was performed under the same conditions while reversing the exposed side of GFs so that a homogenous deposition could be achieved on the fiber surface. The coated samples were dried in a vacuum oven at 40 °C for 12 h. The selected experimental conditions have been optimized as reported in previous studies [23,27] in order to maximize the interfacial fiber-matrix adhesion.

The dried fibers were exposed to hydrazine hydrate vapors at 100 °C for 24 h to reduce the GO coating to rGO [28].

Table 1
Physical properties of epoxy resin.

Physical property	Value
Glass transition temperature (T_g)	33 °C
Thermal degradation	340 °C
Tensile strength (σ_y) (MPa)	26.47 ± 4.21
Stress at break (σ_b) (MPa)	19.77 ± 2.26
Strain at break (ε_b) (mm/mm)	0.17 ± 0.04

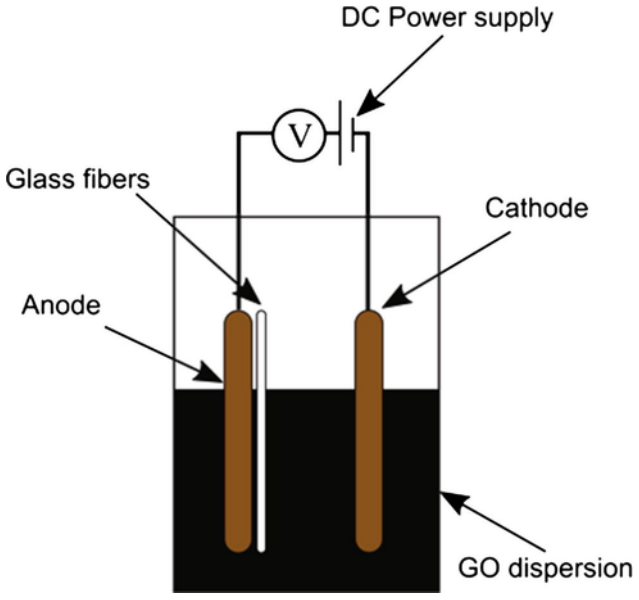

Fig. 1. Schematic diagram of the setup adopted for the electrophoretic deposition of GO nanosheets onto glass fibers. (For interpretation of the references to colour in this figure legend, the reader is referred to the web version of this article.)

2.3. Preparation of GF/rGO/epoxy single fiber model composites

Single rGO coated GF were axially aligned in a silicon mold in which the epoxy resin was poured to fabricate single-fiber model composites for testing the interfacial shear strength (ISS). Pre-curing of the epoxy resin for at least 3 h at room temperature was performed before curing at 60 °C for 15 h. The dimensions of each prismatic cured coupon were 50 mm × 5 mm × 2 mm. The ISS values of bare glass fibers and GO coated single fibers based epoxy composites were investigated under the same conditions in our previous work [23].

2.4. Preparation of hybrid epoxy/glass high fiber volume fraction composites

Hybrid epoxy/glass composites consisting of GO and rGO coated glass fibers were created by hand lay-up method. Briefly, laminates of coated glass fibers were stacked over each other after wetting them with epoxy resin. A constant pressure of 10 kPa was applied on the laminate whose curing was obtained under the conditions described in Section 2.3. The resulting composites had a fiber volume fraction of about 50% as determined by density measurements.

2.5. Testing methods

The oxidation level of pristine graphite, GO and rGO nanosheets was evaluated using X-ray diffraction. Tests were performed using a Rigaku III D-max diffractometer (monochromatic radiation Cu-Kα line with λ = 51.54056 Å) in the 2θ range from 5° to 60° with a step of 0.04°.

A Nikolet Avatar 330 device with a 4 cm^{-1} resolution was used to record Fourier transform infrared (FTIR) spectra. Pristine graphite, GO and rGO powders were individually mixed with potassium bromide (KBr) powder to form homogeneous mixtures and thin discs for analysis were compressed in a metal mold under a pressure of 1 MPa.

Elemental composition of GO and rGO nanosheets was analyzed by X-ray photoelectron spectroscopy (XPS) by a Kratos Axis Ultra DLD machine equipped with a hemispherical analyzer and a monochromatic Al Kα (1486.6 eV) X-ray source. A 90° emission angle between the axis of the analyzer and the sample surface was adjusted. O 1s and C 1s core lines of each sample were collected. The quantification, reported as relative elemental percentage, was performed using the integrated area of the fitted core lines, after Shirley background subtraction, and correcting for the instrument sensitivity factors.

Field emission scanning electron microscopy (FESEM) observations were performed with a Zeiss SUPRA 40 microscope to analyze the morphology and coatings of graphene nanosheets on glass fibers. Approximately 5 nm thick layer of platinum was deposited on samples prior to FESEM observations.

Single-fiber fragmentation test (SFFT) was performed using a small tensile tester (Minimat, by Polymer Laboratories, Loughborough, UK) located under a polarized optical stereo-microscope (Wild M3Z by Leica) to monitor the fiber fragmentation process. Tensile tests were performed at a cross-head speed of 10 mm/min up to a strain of 10% for assuring the saturation of the fragmentation process. The mean fiber length at saturation, L_s, was measured on the optical micrographs by an image analysis software (Image J). A simplified micromechanical model proposed by Kelly and Tyson [34] was utilized to derive the ISS values. According to Kelly and Tyson, a critical fiber length value, L_c, was considered to be 4/3 L_s. The static equilibrium between the tensile force acting on a fiber and the shear force transferred through the fiber-matrix interface allow one to determine an average value of ISS according to the following equation:

$$ISS = \frac{\sigma_{fb}(L_c)d}{2L_c} \tag{1}$$

where d is the fiber diameter and $\sigma_{fb}(L_c)$ is the tensile strength of the fiber at the critical length. This latter value can be estimated by assuming a two-parameters Weibull distribution for the fiber strength, i.e.:

$$\sigma_{fb}(\mathrm{L_C}) = \sigma_0 \left(\frac{\mathrm{L_C}}{\mathrm{L_0}}\right)^{-\frac{1}{\mathrm{m}}} \Gamma\left(1+\frac{1}{m}\right) \tag{2}$$

where σ_0 and m are respectively the scale and shape parameters of the Weibull strength distribution at the reference length L_o, whereas Γ is the Gamma function. These parameters were assessed from tensile tests performed on single fibers. Particularly, single filaments of fiber were extracted from a strand and tested in agreement to the ASTM standard C1557 by using an Instron 4502 universal tensile tester equipped with a 10 N load cell. A gage length of 20 mm was used and 0.2 mm/min of cross-head speed was applied. An iterative procedure originally proposed by Gurvich et al. [35] was used for the data reduction whose outcome is summarized in Table 2.

Table 2
Mechanical properties of glass fiber as determined from single fiber tensile tests.

Parameter	Meaning	Value
N	Number of specimens	31
$\bar{R}$	Average strength at L = 20 mm	2402 MPa
σ_0	Scale parameter of the Weibull distribution	3551 MPa
m	Shape parameter of the Weibull distribution	4.4
υ	Coefficient of variation	26.3%

The following mechanical tests were performed on the laminates by using an Instron 5969 electromechanical testing machine equipped with a 50 kN load cell.

(1) Three-point bending tests were performed according to ASTM D790 on specimens with dimensions of around 80 mm × 13 mm × 1 mm, while the span to depth ratio was fixed at 60:1 and 40:1 for determining flexural modulus and flexural strength, respectively. Therefore, in order to maintain a strain rate of 0.01 mm^{-1}, cross-head speeds of 6.9 mm/min for flexural modulus evaluation and 3.1 mm/min for flexural strength evaluation were respectively adopted.

(2) Short beam shear test was performed according to ASTM D2344 standard. At least 5 specimens 4 mm thick were tested under three-point bending at a cross-head speed of 1 mm/min until a deflection equal to the thickness of the specimen was achieved. The maximum corresponding force (F_m) value was used to evaluate the interlaminar shear strength as:

$$ILSS = 0.75 \times \frac{F_m}{b \times h}$$

(3) Mode I fracture toughness test was performed according to the ASTM 5528 standard. The procedure involved creation of composite specimens consisting of 18 unidirectional laminae with a middle insert of Teflon thin film (thickness = 23 μm) which acted as a crack starter. The final dimensions of the specimen were around 180 mm × 25 mm × 4 mm. Piano hinges were attached to the composite specimen 50 mm apart from the crack tip. The crack advancement during the test was monitored using a digital webcam (Logitech B910 HD) that recorded the video in synchronization with the loading test. Three specimens for each sample were tested at a cross-head speed of 2.5 mm/min and the results were analyzed by considering the following three different criteria. (i) Deviation from linearity (NL) was obtained by considering the point in load-displacement plot where deviation from linearity was observed (or onset of nonlinearity NL), assuming the delamination starts to grow from the insert. (ii) Visual observation (VIS) point where the delamination was visually observed to grow from the insert. (iii) Maximum load (MAX), the highest load measured during the test as obtained from the load-displacement plot.

The short term creep response was investigated by a TA instruments DMA Q800 device in dual cantilever mode. Prismatic specimens of dimensions 55 mm × 13 mm × 1.3 mm were tested under a constant stress (σ_0) of 5 MPa at 30 °C for 3600 s.

Two different methods were employed for resistivity measurement depending on the electrical behavior of the investigated materials. For specimens having electrical resistivity levels exceeding 10^6 Ω cm, the measurements were performed by using a Keithley 8009 resistivity test chamber coupled with a Keithley 6517A high-resistance meter. For more conductive samples, a 6-1/2-digit electrometer/high resistance system (Keithley model 6517A) was used and a 2-points electrical measurement was chosen as test configuration.

3. Results and discussion

3.1. Microstructural characterization

As reported in Fig. 2, X-ray diffraction patterns of precursor graphite show a characteristic and intense peak (0 0 2) at 26.4° thus revealing the crystalline nature of pristine graphite powder. Due to oxidation reaction of graphite powder, the (0 0 2) peak is replaced by a (0 0 1) diffraction peak of GO. The peak shift is due to the increase in interlayer spacing of graphite layers because of insertion of oxygen

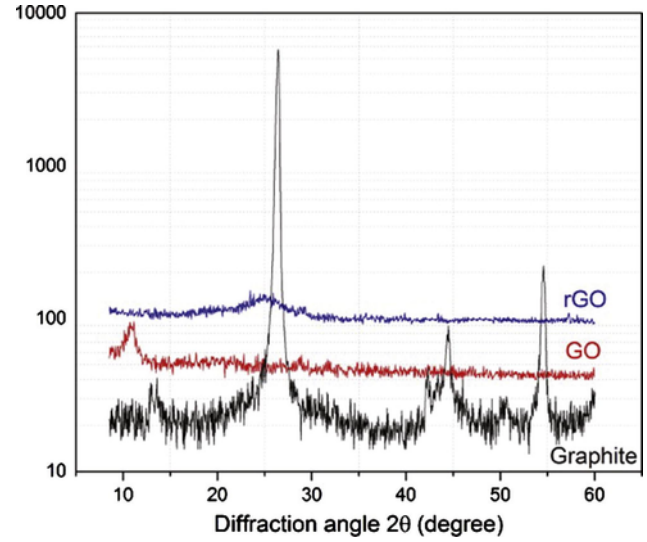

Fig. 2. X-ray diffractograms of graphite, GO and rGO. (For interpretation of the references to colour in this figure legend, the reader is referred to the web version of this article.)

functional groups in GO as well as water molecules [29,30]. Finally, the rGO diffractogram manifests a peak repositioned back to the pristine graphite peak location due to the removal of most of the oxygen groups from GO, hence decreasing the interlayer spacing. Note that both GO and rGO peaks are less intense and broader due to amorphous/distorted nature hence confirming exfoliation.

FTIR spectra of graphite, GO and rGO are reported in Fig. 3. As compared to pristine graphite, GO shows relatively intense peaks of groups like epoxy C—O (at 1085 cm^{-1}), C═O (at 1625 cm^{-1}) and O—H (at 3830 cm^{-1}) that confirms the destruction of original extended conjugated π-orbital system of the graphite and insertion of oxygen-containing functional groups into carbon skeleton [31]. However, after chemical reduction, a lowering in the intensity of the functional groups peaks of rGO spectra can be observed, hence confirming the partial removal of oxygen-containing groups.

Fig. 4 shows the XPS spectra of both GO and rGO samples. In brief, the C 1s XPS spectrum of GO indicates a certain degree of oxidation with at least three components of oxygen functional groups attached to carbon: the carboxyl group (COOH), the C in C—O bonds and non-oxygenated carbon (C—C). The semi-qualitative results for

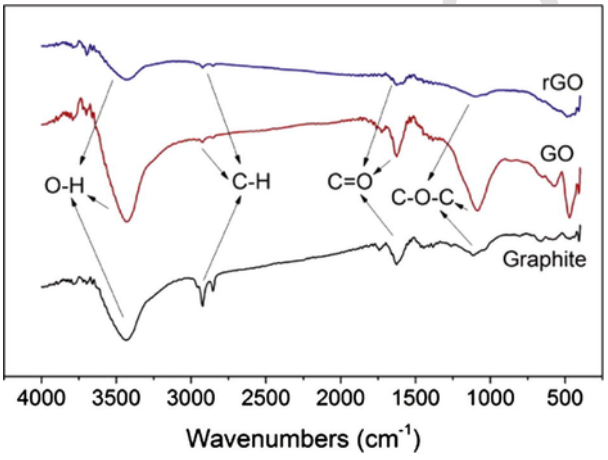

Fig. 3. Fourier transform infrared (FTIR) spectra of graphite, GO and rGO.

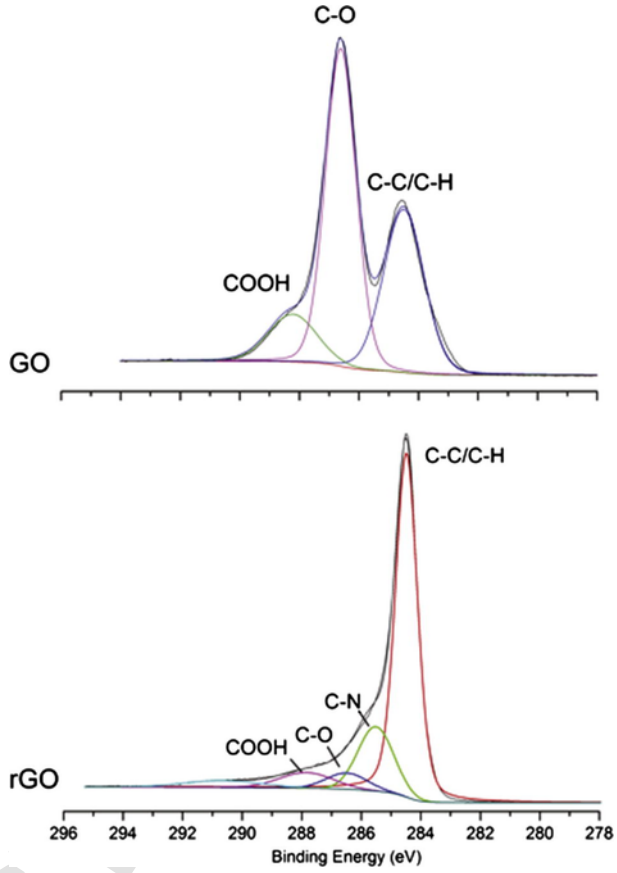

Fig. 4. The C1s XPS spectra of GO and rGO. (For interpretation of the references to colour in this figure legend, the reader is referred to the web version of this article.)

the carbon and oxygen present on the specimen surface were also calculated using the atomic sensitivity factors which showed oxygen and carbon levels of 34% and 66% respectively (Table 3). XPS spectrum of rGO also displays the same functional groups present in the sample however the difference is the reduced intensity of peaks of oxygenated groups while the non-oxygenated carbon group had a higher intensity. The presence of a new group such as C—N in rGO spectrum is related to the fact that the chemical reduction of GO was obtained by exposure to hydrazine hydrate vapors having nitrogen as a key element. After chemical reduction, the amount of oxygen in rGO decreases to 9.9% (Table 3).

SEM pictures reported in Fig. 5 display the surfaces of GF fibers extracted from a bundle before (Fig. 5a) and after (Fig. 5b) EPD coating with GO and subsequent chemical reduction of the coating to rGO (Fig. 5c) nanosheets. Fig. 5b and c clearly show that the glass fibers are completely covered with GO and rGO nanosheets thus confirming the efficacy of the proposed electrophoretically deposition method [23,32].

A detailed study of the interaction between a coating of GO electrophoretically deposited onto E-glass and subsequently reduced into rGO by exposure to hydrazine hydrate at 100 °C fiber has been re-

Table 3
Elemental analysis of GO and rGO specimens as obtained from XPS analysis.

Sample	O (%)	C (%)
GO	34.2	65.8
rGO	9.9	90.1

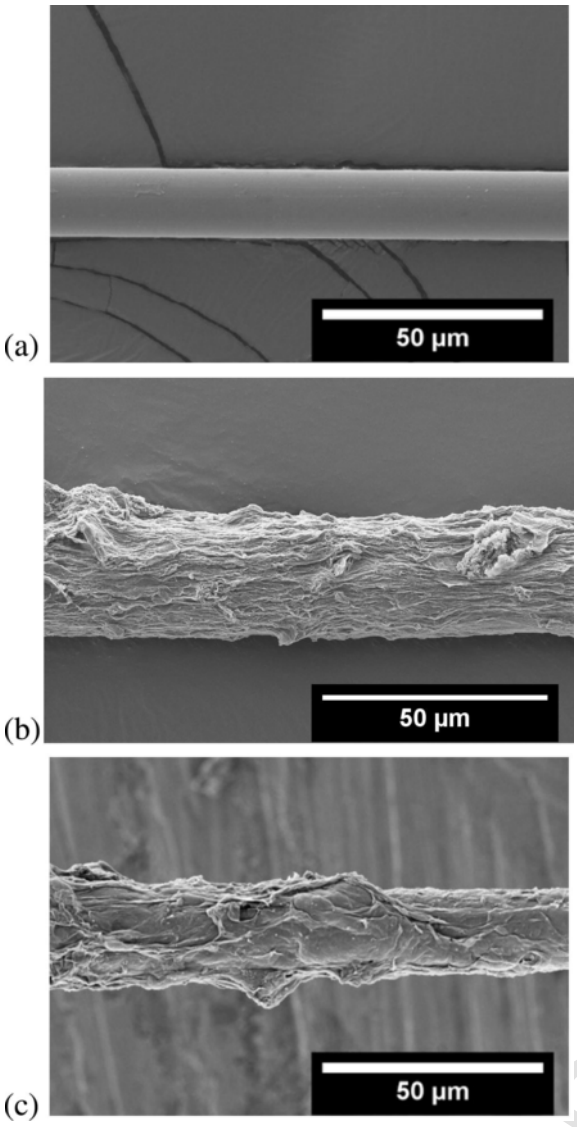

Fig. 5. Scanning electron microscopy images of (a) bare glass fiber and (b) glass fiber coated with GO and (c) glass fiber coated with rGO.

cently performed [33]. Treatment with hydrazine hydrate reduces adhesion and friction force against diamond like carbon coated Si probe (DLC AFM) at the basal plain of the coatings. Investigation at the edges revealed that the presence of oxygen functional group leads to higher shear strength with glass-fiber which reduces after treatment with hydrazine.

3.2. Fiber-matrix adhesion in single-fiber model composites

The average values of fiber's fragment lengths measured in SFFT and subsequent calculations of ISS for rGO coated glass fibers epoxy composite and their comparison with uncoated and GO coated glass fiber epoxy composites are reported in Table 4. rGO coated fibers show a decrease of the fragments length at saturation as compared to uncoated ones. This naturally brings to estimate higher ISS values. ISS values measured with both GO and rGO coated fibers are higher than those obtained with uncoated GF. The enhancement of ISS for GO and rGO coated fibers as compared to uncoated fiber could be attributed to the fact that both GO and rGO contain functional groups

Table 4
Comparison of ISS values according to Kelly–Tyson model as determined by average fragment length and tensile strength of fiber for uncoated [23], GO coated [23] and rGO coated fibers composites.

Fiber condition	Average fragment length, L_s (mm)	Critical length, L_c (mm)	Fiber strength at the critical length, $\sigma_{fb}(L_c)$ (MPa)	Interlaminar shear strength, ISS (MPa)
Uncoated	2.7±0.9	3.5±1.2	3548.2±267.5	9.0±3.5 [23]
GO coated	0.9±0.1	1.3±0.1	4436.0±111.9	28.6±3.9 [23]
rGO coated	1.6±0.3	2.1±0.4	3940.9±167.9	15.2±3.7

which provide a possibility of favorable bond between the GFs and epoxy resin which eventually enhances the effective distribution of load on the GF. Another reason for an increase in ISS could be the increased surface roughness and the good adhesive compatibility between the epoxy matrix and the deposited coatings which promote mechanical interlocking. An important fact to be considered here is that this 70% increase observed for rGO coated fibers is lower than the previously reported increment percentage in case of GO coating [23]. This is due to the fact that rGO contains less functional groups which play a major role for a better adhesion and consequently improved load transfer mechanisms [34].

3.3. Mechanical behavior of unidirectional composites

Typical flexural stress-strain curves of the multiscale composites are reported in Fig. 6. It can be observed that the presence of both GO and rGO interphase improve the composites behavior. Fig. 7 shows the resulting flexural modulus and flexural strength values. The flexural modulus increases by 19% and 9% for GO and rGO coated GF, respectively, as compared to neat composites. The increase in modulus is related to the fact that GO interphase between the matrix and the fibers improved the bonding conditions and mechanical interlocking phenomena [23]. The flexural strength of the composites containing GO shows an increase by 20%, again due to the better interfacial adhesion, but in case of rGO, the value is practically the same as compared to uncoated fiber based composites.

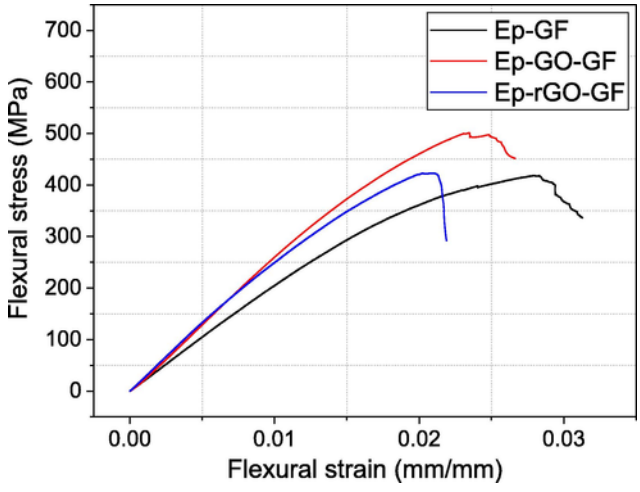

Fig. 6. Typical flexural stress-strain curves of unidirectional composites with uncoated, GO coated and rGO coated glass fibers. (For interpretation of the references to colour in this figure legend, the reader is referred to the web version of this article.)

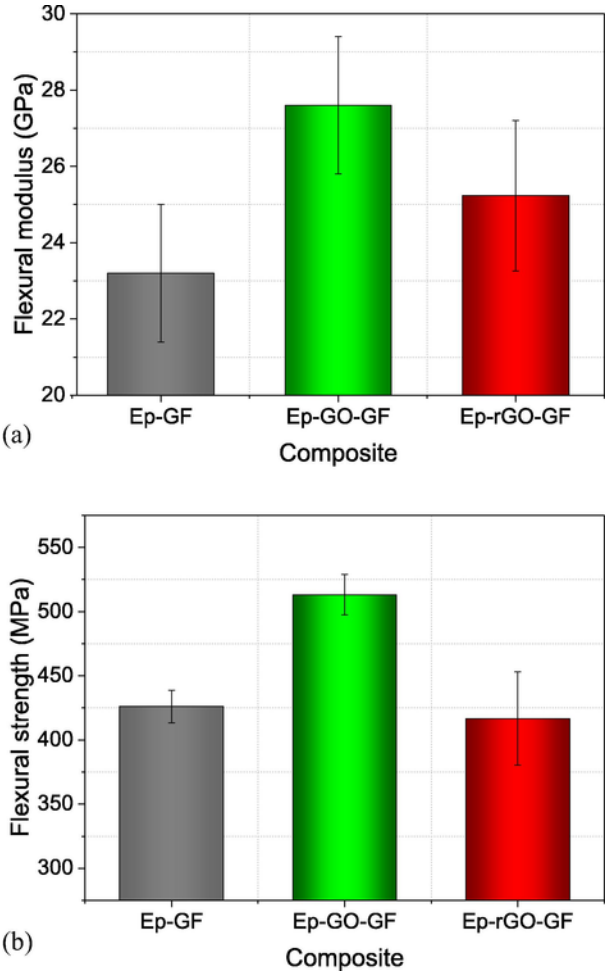

Fig. 7. (a) Flexural modulus and (b) flexural strength as determined by three-point bending tests on unidirectional composites with uncoated, GO coated and rGO coated glass fibers. (For interpretation of the references to colour in this figure legend, the reader is referred to the web version of this article.)

Interlaminar shear strength (ILSS) values of the composites was investigated by the short beam shear and the obtained values are reported in Fig. 8. The epoxy/glass composites with a GO interphase reach a 15% increase in the ILSS as compared to composites with uncoated fibers while a 9% increase is found for rGO based glass/epoxy composites. This result also supports previous observations in which GO coated fibers offer dual reinforcing phenomena i.e. oxygen-based functional groups and mechanical interlocking together bridging the epoxy and glass fibers in the composite [23]. This "cross-linking" via the interface causes an enhancement in interfacial strength, which can be inferred as an evidence for the enhanced ILSS values. In case of rGO coated fibers, the main reinforcing mechanism is the mechanical interlocking which promotes an increase of ILSS but not at the levels observed for GO coated fibers. Again, the observed differences can be attributed to the lower amount of oxygen-based functional groups on the surface of rGO in comparison of rGO coated fibers. The images of the composite specimens failed during short beam shear test are reported in Fig. 9 where the interlaminar failure can be clearly noticed. It is interesting to observe that the composite with rGO coated fibers (Fig. 9c) presents more shear cracks between the laminae.

In case of Mode I fracture toughness tests, the strain energy release rate values for each composite are evaluated from the load-displacement plot of Fig. 10a and plotted as resistance curves (R-curves)

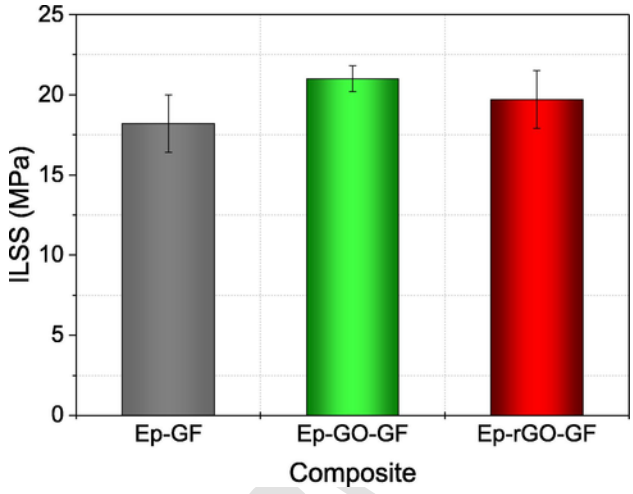

Fig. 8. Interlaminar shear strength (ILSS) values as obtained from the short beam shear tests performed on unidirectional composites with uncoated, GO coated and rGO coated glass fibers. (For interpretation of the references to colour in this figure legend, the reader is referred to the web version of this article.)

as shown in Fig. 10b. Table 5 shows the average values of the three composites tested. An explanation of the obtained G_{Ic} values can be best provided by a comparison with the ILSS values as obtained from the short beam shear test. As it can be seen in Fig. 10c, composites reinforced with GO coated GF showed the highest values for the NL and VIS G_{Ic} values as compared to uncoated GF and rGO coated GF. The G_{Ic} values computed according to the MAX procedure are however practically the same for the composites. rGO coated GF fibers also provide some resistance to crack propagation but less than GO coating, which is pretty comparable to the result of ILSS. This investigation clearly shows the higher energy required for crack propagation when GO is deposited on GF as a continuous reinforcing interphase in epoxy/glass composites.

Interesting observations were obtained during the analysis of the fracture surfaces obtained after mode I fracture toughness test of DCB specimens. The fracture surfaces of Ep-GF composite (Fig. 11a) indicate a weak fiber-matrix interaction revealed by the presence of the glass fibers with a clean surface. On the other hand, the fracture surfaces of Ep-GO-GF (Fig. 11b) shows a number of fibers coated with the remnants of epoxy matrix which could be associated to a good interfacial adhesion. It can be visualized from the FESEM images that the fibers are bonded together with continuous epoxy resin hence suggesting the influence of GO coating on fibers promoting strong inter-fiber interactions due to epoxy/GO/GF system. At the end, the fracture surfaces obtained from the Ep-rGO-GF composite system gives a different picture in which the fiber surfaces are covered totally with a continuous coating (Fig. 11c). A detail examination reveals that the rGO coating had a different morphology as compared to the epoxy matrix. The lower values of NL during mode I fracture toughness is a clear evidence that debonding took place at the epoxy/rGO interface. This is correlated to the fact that rGO sheets, due to unavailability of the oxygen based functional groups, offered a weaker interfacial adhesion towards the epoxy matrix.

The improvement in mechanical properties obtained in this work are summarized in Table 6 in which the results are also compared with recent work done for improving similar properties in other systems. It can be seen that the trend involves the use of graphene as an interphase thus creating a synergistic effect of improving of mechanical properties by the combination of chemical bonding plus mechanical interlocking between the matrix and the fiber.

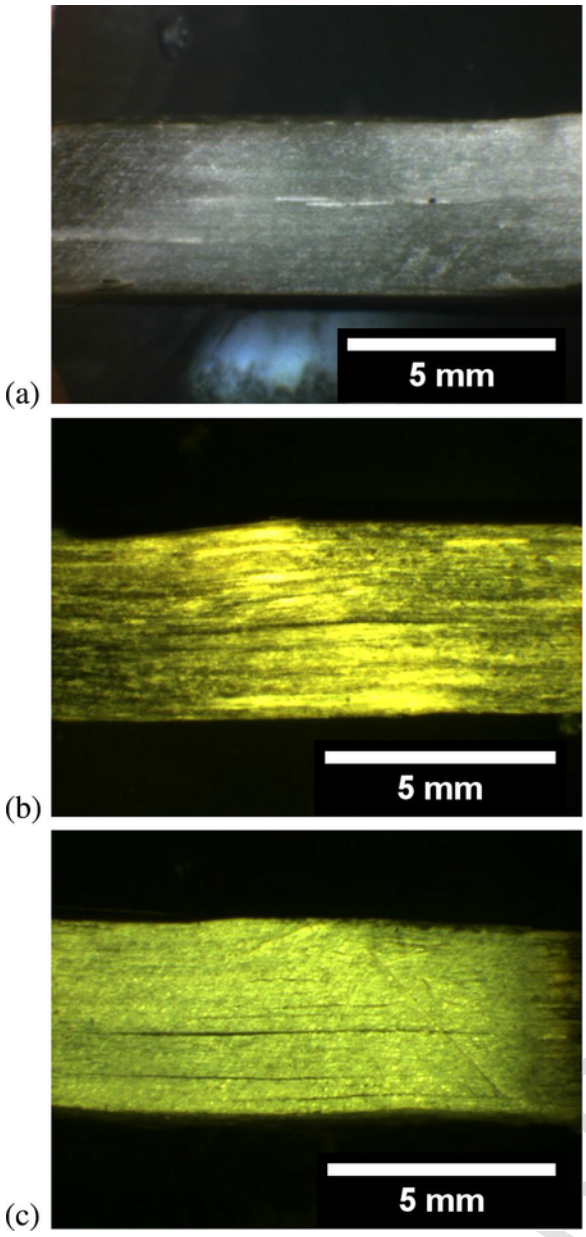

Fig. 9. Optical microscopy images of composite specimens (side view) after being subjected to short beam shear tests: composites with (a) uncoated, (b) GO coated and (c) rGO coated glass fibers. (For interpretation of the references to colour in this figure legend, the reader is referred to the web version of this article.)

Isothermal creep compliance curves of the unidirectional composites with uncoated, GO coated and rGO coated glass fibers at a reference temperature of 30 °C and applied stress of 5 MPa are shown in Fig. 12 while the values of the instantaneous creep compliance (De), of the viscoelastic component after 2000 s (D_{ve2000}) and of the total creep compliance after 2000 s (D_{t2000}) are reported in Table 7. A significant reduction of the creep compliance can be noticed for composites reinforced with GO and rGO coated fiber as compared to reference composite with uncoated fibers. This improvement in the creep stability is the consequence of a remarkable reduction of both the elastic and the viscoelastic components of the total creep compliance.

Findley's model was adopted to fit the experimental data obtained through creep testing. This model can be obtained by expanding the Kohlrausch–Williams–Watts (KWW) model, generally described by a Weibull-like function as a series and ignoring all but the first term [35]:

$$D(t) = D_0 + k(t)^n \quad (1)$$

where D_0 is the elastic instantaneous creep compliance, k is a coefficient related to the magnitude of the underlying retardation process and n is an exponent tuning the time dependency of the creep process. D_0 and k are functions of environmental variables. In this work, creep curves at different temperatures for different composites were fitted using Findley's model to investigate possible correlations between the viscoelastic response of the material and the fitting parameters. The creep compliance curves of the investigated composites have been tentatively fitted with the Findley model (Eq. (1)), and the results are shown in Fig. 12. The parameters obtained from the best fitting of experimental creep data are summarized in Table 7, along with R^2 values. It can be noticed that the Findley model successfully fits all the creep curves, with R^2 values of around 0.99 for all the cases. It is interesting to observe that, as compared to neat composites, the reduction of the creep compliance due to the presence of the GO coating in Ep-GO-GF composites results in a substantial reduction of the instantaneous creep compliance term D_e and of the coefficient k, related to the strain retardation process of the macromolecules. Moreover, the parameter n was not changed by the GO coating of the GF as compared to the uncoated GF based epoxy composite. For Ep-rGO-GF composite, however, there was a slight increase of the D_e as compared to the neat composite and at the same time the coefficient k drops very significantly, which shows that the retardation of creep process increases tremendously afterwards.

3.4. Electrical resistivity and piezoresistivity behavior

Three different composites were tested for their electrical resistivity as shown in Fig. 13. In case of uncoated glass fibers/epoxy composite (GF/Ep), the volume resistivity is in the range of $10^{14}\,\Omega\,cm$ which is a typical value for insulating epoxy/glass composites. When composites are prepared by using glass fibers coated with GO only a small decrease of the electrical resistivity is observed with volume resistivity value in the range of $10^{13}\,\Omega\,cm$, this being due to the insulating nature of GO [36]. However, for the composite with an rGO interphase a volume resistivity value as low as $10^{2}\,\Omega\,cm$ can be measured. The massive drop in resistivity thus confirms the reduction of GO and hence making the graphene sheets conductive.

The piezoresistive response of GF/rGO/Ep composites was monitored on composite specimens subjected to mechanical loading and a simultaneous measure of electrical resistance by two points contact. Figs. 14–17 show the dependence of electrical resistance on the applied strain (or stress) for the GF/rGO/Ep composites under various loading modes. In case of quasi-static tensile mode (as schematically depicted in Fig. 14a), it is interesting to observe that within the initial 0.1% strain (Fig. 14b), the electrical resistance decreases which could be attributed to the rearrangement of the coated fibers at the microscale hence a possibility of having better electrical coupling among each other consequently a decrease in resistance. At higher strain levels, the change in resistance increases steadily till it became steep after 0.2% tensile strain. Considering this, a tangent line in this elastic portion provide a gage factor of about 11 by the formula $(k = (\Delta R/R_0)/\varepsilon)$. Since the Poisson's ratio of the analyzed composite was 0.36 (as measured by a biaxial extensometer), the contribution of the geometric part can be estimated to be of about 0.01.

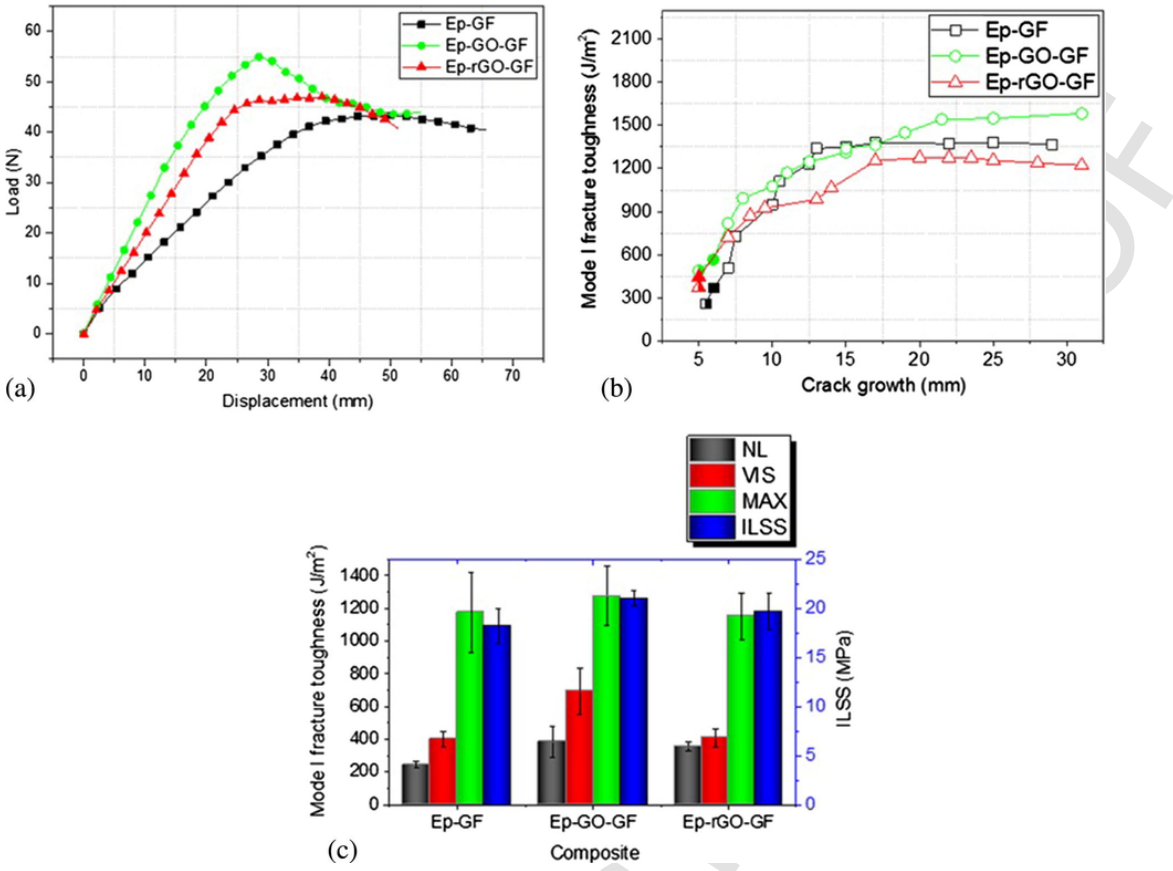

Fig. 10. (a) Typical load-displacement curves obtained under mode I fracture toughness tests of investigated composites. (b) Delamination resistance curves (R-curves) where half-filled symbols represent NL (Non linearity) and solid symbols represent VIS (visual observation). (c) Comparison between mode I fracture toughness values (NL: non-linear, VIS: visual observation, MAX: maximum load, ILSS: interlaminar shear strength) and short beam shear strength. (For interpretation of the references to colour in this figure legend, the reader is referred to the web version of this article.)

Table 5
Mode I fracture toughness (G_{Ic}) values of Ep-GF, Ep-GO-GF and Ep-rGO-GF composites.

Specimen	Nonlinearity (NL)	Visual observation (VIS)	Maximum load (MAX)
	(J/m^2)	(J/m^2)	(J/m^2)
Ep-GF	243.5±21.5	401.8±46.3	1176.4±244.9
Ep-GO-GF	384.3±92.6	692.9±145.1	1275.8±180.5
Ep-rGO-GF	352.8±27.0	407.9±52.8	1153.2±141.7

Fig. 15a shows the schematic diagram of the flexural test wherein the piezoresistivity was monitored on the bottom side of the specimen which experiences the tensile stresses. In Fig. 15b the piezoresistivity response of the specimen's surface under tensile stress is reported. The piezoresistivity on this surface could be visualized when considering the influence of stresses acting on the fibers. A steady resistance change can be observed till 2.5% of flexural strain, the resistance change was steady until the fibers started to break resulting in failing of the specimen which consequently had a dramatic effect on the relative change of resistance. Similar kind of behavior can be also observed from the analysis of the compressive side of the specimen (Fig. 15c, d).

In another testing protocol, the reversibility of electrical network was tested by subjecting the hybrid composite specimen under repeated loading-unloading cycles in the strain range of $0.1\% < \varepsilon < 0.5\%$ and the electrical resistance was monitored during each loading and unloading part of the cycle. Fig. 16 shows the results obtained under cyclic tensile conditions in which the reversible piezoresistivity can be confirmed. The gage factor calculated here was about 3.8. A similar test method was also applied to load a specimen under cyclic flexural mode under load control (0–25 MPa). As shown in Fig. 17, the piezoresistive behavior the multiscale composite is also replicated in flexural mode which confirms the rGO coating on GF can provide the possibility of a strain monitoring based on the control of the electrical resistance variations.

4. Conclusions

GO was successfully deposited on GF using electrophoretic deposition technique and subsequently reduced to rGO using hydrazine hydrate at 100 °C for 24 h. XPS analysis evidenced a reduction of the oxygen content from 34.2% of GO to 9.9% of rGO. The obtained rGO coating appeared to be quite uniform across a length of fiber.

Fiber-matrix interfacial adhesion evaluated by single fiber fragmentation test on epoxy matrix showed a +70% increase in ISS of rGO based epoxy/glass composites as compared to uncoated GF based composites. This ISS is lower than the increase (+218%) measured on composites with GO coated fibers due to less oxygen based functional groups attached with rGO nanosheets. Mechanical test (three-point bending, short beam shear and mode-I fracture toughness) on high fiber volume fraction composites revealed that GO coted fibers lead to an increase of elastic modulus, stress at break and

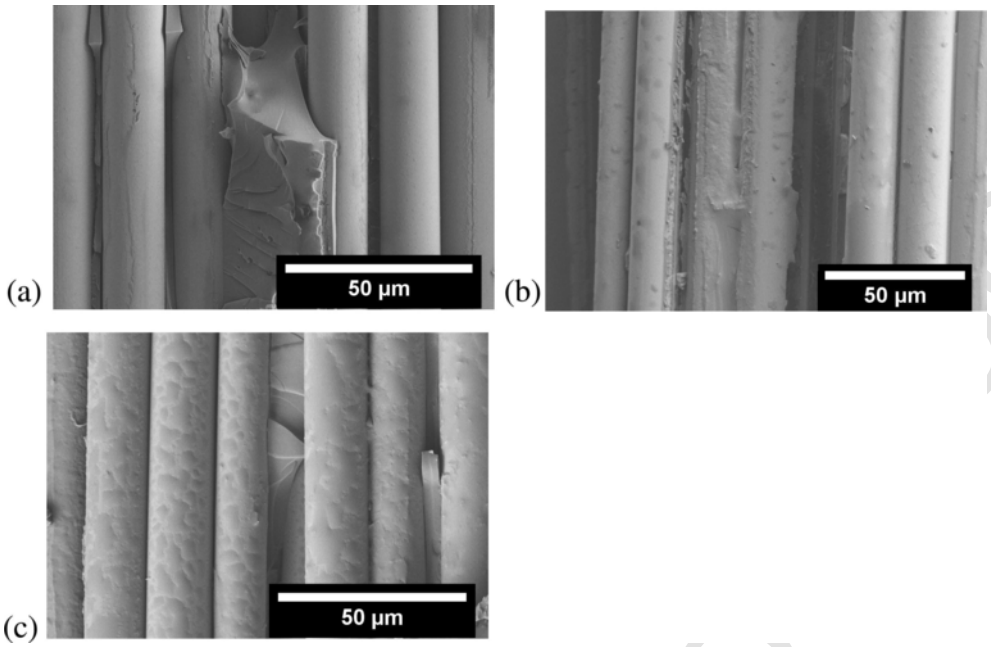

Fig. 11. Fracture surfaces of composites obtained during Mode I fracture toughness test as observed by FESEM (crack propagation from top to bottom) where a) Ep-GF, b) Ep-GO-GF and c) Ep-rGO-GF.

Table 6

Fiber type with coating	Coating/Deposition process	Mechanical improvement	Interphase bonding phenomenon	Reference
Current work	EPD	IFSS = Improvement of ~217% for GO, Improvement of ~70% for rGO; ILSS = 15% improvement for GO and improvement of 9% for rGO; Flexural properties = ~20% improvement in modulus and strength for GO	Covalent bonding + mechanical interlocking	
Carbon fiber (CF) coated by silanized GO	Dipping	IFSS = 60% improvement; ILSS = 19% improvement; Flexural strength, modulus by 15%	Van der Waals + chemical bonding	[37]
GF coated by GO	Grafting via covalent immobilization	ILSS = 41% improvement	Mechanical locking + covalent bonding	[22]
CF coated with GnP	Solution coating process	Flexural strength increase by 82%; ILSS improvement by 19%	Failure mode: hybrid interfacial/ cohesive + mechanical interlocking	[38]
CF (sized) coated with functionalized GO	Grafting	ILSS = 53% improvement	chemical bonding at the interface	[39]
CF coated with GO	Tandem oxidation-ultrasonically assisted EPD	ILSS = 56% improvement	Hydrogen bonding at the interface	[40]
CF coated with GO	Epoxy/GO sizing	IFSS = 70.9% improvement; ILSS = 12.7% improvement	Chemical bonding at the interface	[41]

interlaminar shear strength, while composites with rGO coated fibers perform similarly to composites with uncoated fibers. In addition, short term creep tests revealed how a graphene-based interphase offers excellent resistance to creep deformation.

Finally, composites possessing rGO interphase manifested low resistivity values due to the conductive nature of rGO nanosheets. Piezoresistivity of the rGO based composites was verified by applying various loading conditions and simultaneously measuring changes in electrical resistance hence confirming the applicability of such composites for strain monitoring in structural applications.

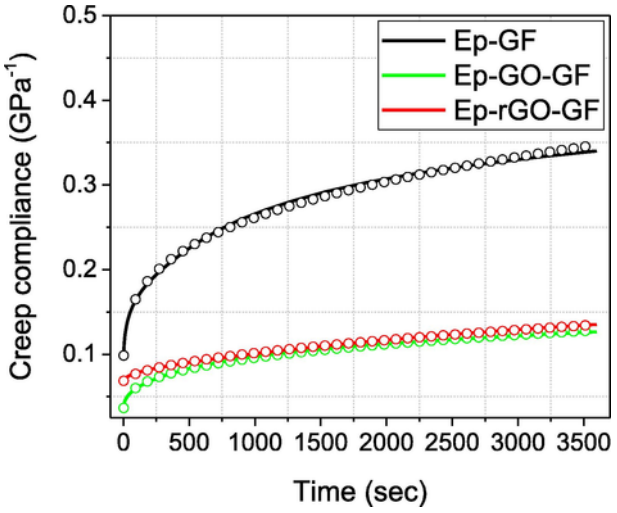

Fig. 12. Experimental creep compliance curves (solid line) of the investigated composites and theoretical prediction (open circles) according to the Findley model (T = 30 °C, σ = 5 MPa). (For interpretation of the references to colour in this figure legend, the reader is referred to the web version of this article.)

Table 7
Creep compliance components and their fitting parameters of the composites Ep-GF, Ep-GO-GF and Ep-rGO-GF (T = 30 °C, σ = 5 MPa).

	Creep compliance parameters			Fitting parameters (Findley's model)			
	D_e (GPa^{-1})	D_{ve2000} (GPa^{-1})	D_{t2000} (GPa^{-1})	D_e (GPa^{-1})	K ($GPa^{-1} s^{-n}$)	n	R^2
Ep-GF	0.094	0.213	0.307	0.064	0.028	0.3	0.99832
Ep-GO-GF	0.035	0.077	0.112	0.025	0.009	0.3	0.99882
Ep-rGO-GF	0.064	0.053	0.117	0.067	0.0008	0.5	0.99745

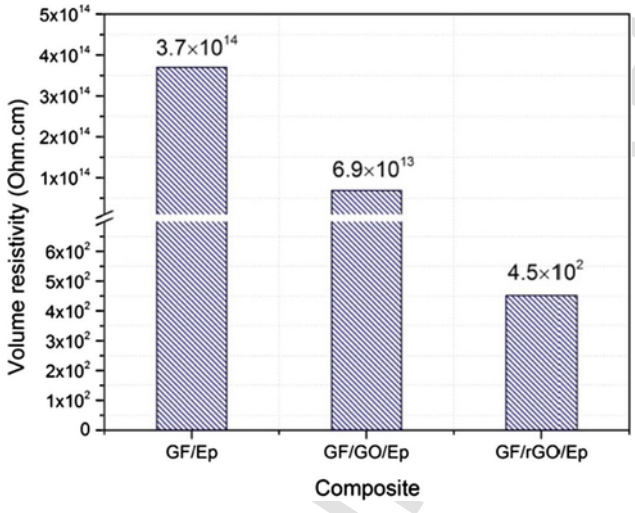

Fig. 13. Volume resistivity of the unidirectional composites with uncoated, GO coated and rGO coated glass fibers. (For interpretation of the references to colour in this figure legend, the reader is referred to the web version of this article.)

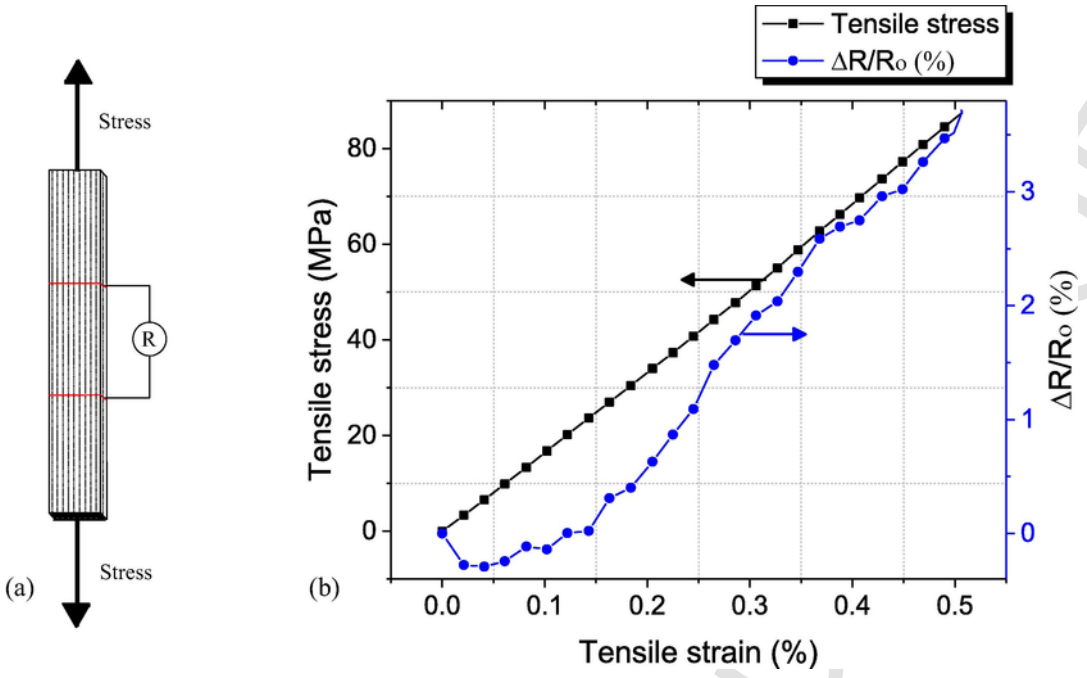

Fig. 14. (a) Schematic of testing setup for piezoresistivity tests under tensile mode, (b) piezoresistivity response of unidirectional composites with rGO coated glass fibers under tensile loading condition. (For interpretation of the references to colour in this figure legend, the reader is referred to the web version of this article.)

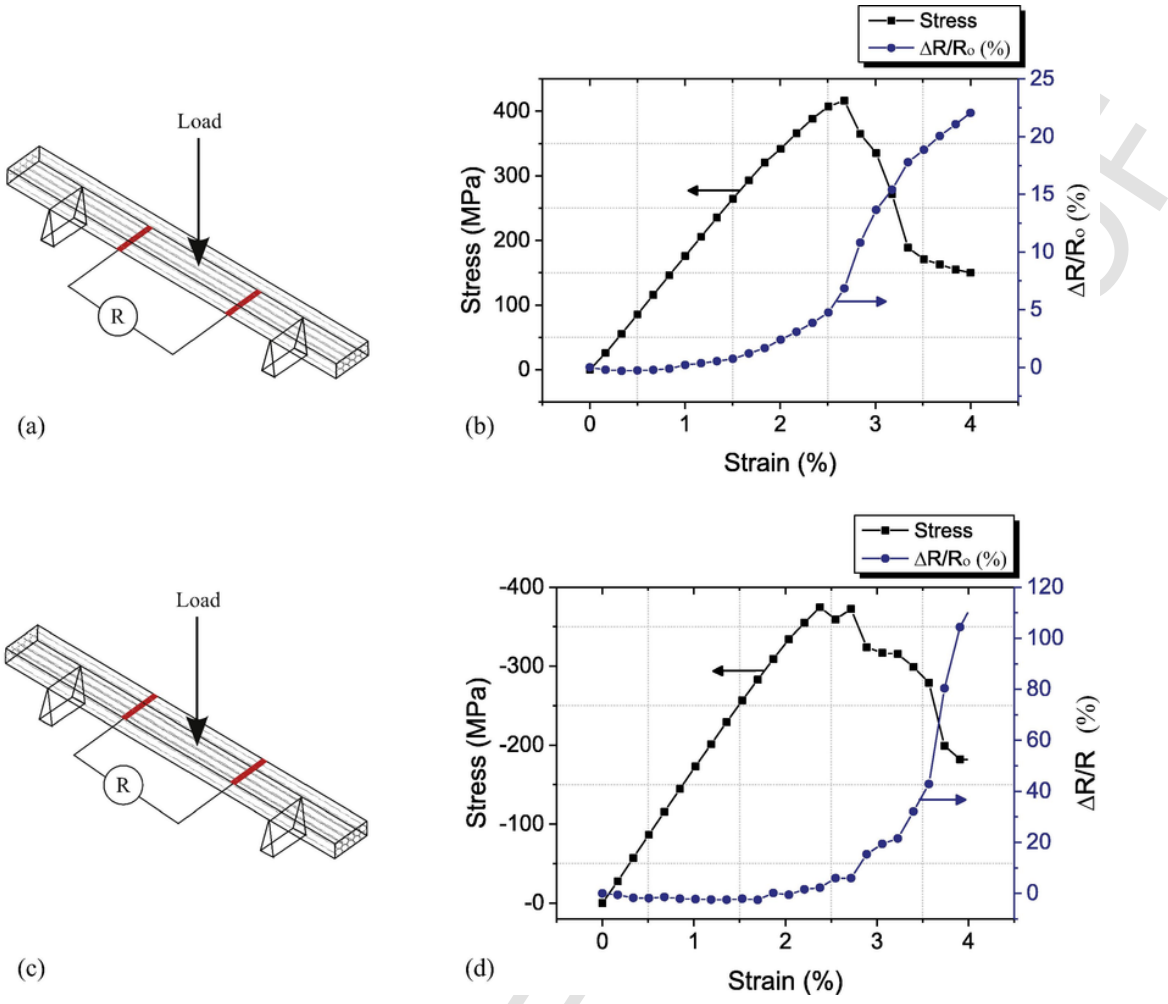

Fig. 15. Schematic of testing setup for piezoresistivity tests under flexural mode where change in resistance was monitored on the surfaces experiencing (a) tensile and (c) compressive stresses, respectively. Piezoresistivity response of unidirectional composites with rGO coated glass under on the (b) tensile and (d) compressive sides of the specimens. (For interpretation of the references to colour in this figure legend, the reader is referred to the web version of this article.)

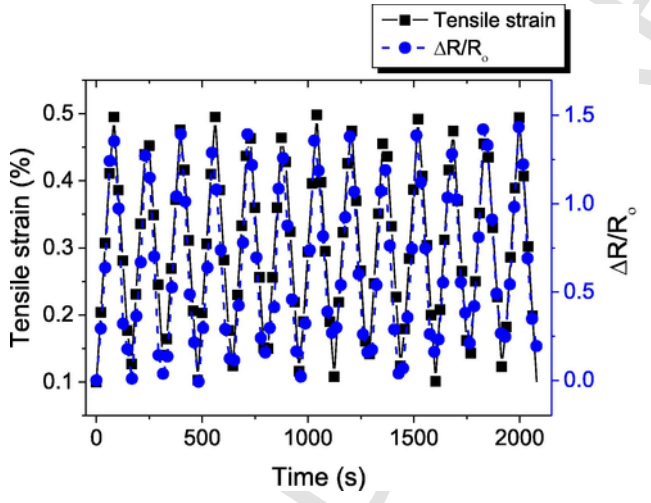

Fig. 16. Piezoresistivity response of unidirectional composites with rGO coated glass fibers under tensile cyclic tests under strain control. (For interpretation of the references to colour in this figure legend, the reader is referred to the web version of this article.)

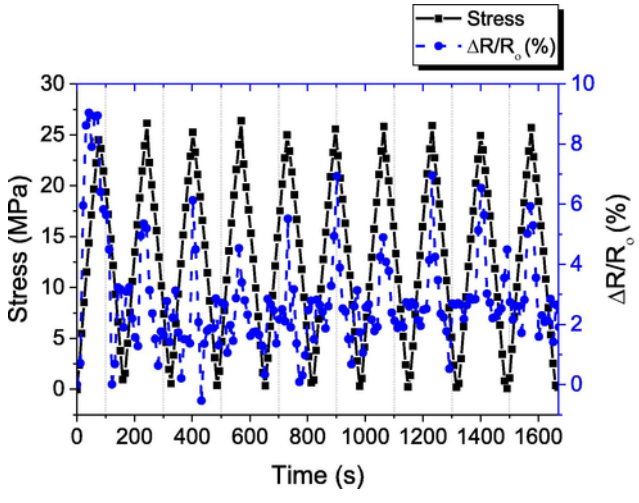

Fig. 17. Piezoresistivity response of unidirectional composites with rGO coated glass fibers under flexural cyclic tests under load control. (For interpretation of the references to colour in this figure legend, the reader is referred to the web version of this article.)

References

[1] A. Pegoretti, J. Karger-Kocsis, Interphase engineering in polymer composites: challenging the devil, eXPRESS Polym Lett 9 (10) (2015) 838.
[2] F.R. Jones, A review of interphase formation and design in fibre-reinforced composites, J Adhes Sci Technol 24 (1) (2010) 171–202.
[3] J. Karger-Kocsis, H. Mahmood, A. Pegoretti, Recent advances in fiber/matrix interphase engineering for polymer composites, Prog Mater Sci 73 (2015) 1–43.
[4] R.K. Gupta, E. Kennel, K.-J. Kim, Polymer nanocomposites handbook, CRC Press, Boca Raton, FL, 2010.
[5] X. Sun, H. Sun, H. Li, H. Peng, Developing polymer composite materials: carbon nanotubes or graphene?, Adv Mater 25 (37) (2013) 5153–5176.
[6] K. Inpil, J.S. Mark, H.K. Jay, S. Vesselin, S. Donglu, A carbon nanotube strain sensor for structural health monitoring, Smart Mater Struct 15 (3) (2006) 737.
[7] W. Zhang, J. Suhr, N. Koratkar, Carbon nanotube/polycarbonate composites as multifunctional strain sensors, J Nanosci Nanotechnol 6 (4) (2006) 960–964.
[8] L. Böger, M.H.G. Wichmann, L.O. Meyer, K. Schulte, Load and health monitoring in glass fibre reinforced composites with an electrically conductive nanocomposite epoxy matrix, Compos Sci Technol 68 (7–8) (2008) 1886–1894.
[9] R. Moriche, M. Sánchez, A. Jiménez-Suárez, S.G. Prolongo, A. Ureña, Strain monitoring mechanisms of sensors based on the addition of graphene nanoplatelets into an epoxy matrix, Compos Sci Technol 123 (2016) 65–70.
[10] R. Moriche, M. Sánchez, S.G. Prolongo, A. Jiménez-Suárez, A. Ureña, Reversible phenomena and failure localization in self-monitoring GNP/epoxy nanocomposites, Compos Struct 136 (2016) 101–105.
[11] A.C. Ferrari, F. Bonaccorso, V. Fal'ko, K.S. Novoselov, S. Roche, P. Boggild, et al., Science and technology roadmap for graphene, related two-dimensional crystals, and hybrid systems, Nanoscale 7 (11) (2015) 4598–4810.
[12] K.S. Novoselov, A.K. Geim, S.V. Morozov, D. Jiang, Y. Zhang, S.V. Dubonos, et al., Electric field effect in atomically thin carbon films, Science 306 (5696) (2004) 666–669.
[13] C. Lee, X. Wei, J.W. Kysar, J. Hone, Measurement of the elastic properties and intrinsic strength of monolayer graphene, Science 321 (5887) (2008) 385–388.
[14] A.A. Balandin, S. Ghosh, W. Bao, I. Calizo, D. Teweldebrhan, F. Miao, et al., Superior thermal conductivity of single-layer graphene, Nano Letters 8 (3) (2008) 902–907.
[15] T. Kuilla, S. Bhadra, D. Yao, N.H. Kim, S. Bose, J.H. Lee, Recent advances in graphene based polymer composites, Prog Polym Sci 35 (11) (2010) 1350–1375.
[16] S. Park, J. An, I. Jung, R.D. Piner, S.J. An, X. Li, et al., Colloidal suspensions of highly reduced graphene oxide in a wide variety of organic solvents, Nano Lett 9 (4) (2009) 1593–1597.
[17] S. Stankovich, D.A. Dikin, R.D. Piner, K.A. Kohlhaas, A. Kleinhammes, Y. Jia, et al., Synthesis of graphene-based nanosheets via chemical reduction of exfoliated graphite oxide, Carbon 45 (7) (2007) 1558–1565.
[18] L. Chang, K. Friedrich, Enhancement effect of nanoparticles on the sliding wear of short fiber-reinforced polymer composites: a critical discussion of wear mechanisms, Tribol Int 43 (12) (2010) 2355–2364.
[19] D. Pedrazzoli, A. Pegoretti, Expanded graphite nanoplatelets as coupling agents in glass fiber reinforced polypropylene composites, Compos A Appl Sci Manuf 66 (2014) 25–34.
[20] D.P.N. Vlasveld, P.P. Parlevliet, H.E.N. Bersee, S.J. Picken, Fibre–matrix adhesion in glass-fibre reinforced polyamide-6 silicate nanocomposites, Compos A Appl Sci Manuf 36 (1) (2005) 1–11.
[21] A. Dorigato, A. Pegoretti, M. Quaresimin, Thermo-mechanical characterization of epoxy/clay nanocomposites as matrices for carbon/nanoclay/epoxy laminates, Mat Sci Eng A-Struct 528 (19–20) (2011) 6324–6333.
[22] J. Chen, D. Zhao, X. Jin, C. Wang, D. Wang, H. Ge, Modifying glass fibers with graphene oxide: towards high-performance polymer composites, Compos Sci Technol 97 (2014) 41–45.
[23] H. Mahmood, M. Tripathi, N. Pugno, A. Pegoretti, Enhancement of interfacial adhesion in glass fiber/epoxy composites by electrophoretic deposition of graphene oxide on glass fibers, Compos Sci Technol 126 (2016) 149–157.
[24] Ali MA, Umer R, Khan KA, Samad YA, Liao K, Cantwell W. Graphene coated piezo-resistive fabrics for liquid composite molding process monitoring. Compos Sci Technol 2017;148(Suppl. C):p. 106–14.
[25] Moriche R, Jiménez-Suárez A, Sánchez M, Prolongo SG, Ureña A. Graphene nanoplatelets coated glass fibre fabrics as strain sensors. Compos Sci Technol 2017;146(Suppl. C):p. 59–64.
[26] Hummers WS, Offeman RE. Preparation of Graphitic Oxide. Journal of the American Chemical Society. 1958;80(6):1339-.
[27] A. Pegoretti, H. Mahmood, D. Pedrazzoli, K. Kalaitzidou, Improving fiber/matrix interfacial strength through graphene and graphene-oxide nano platelets, IOP Conf Ser: Mater Sci Eng 139 (2016) 1–12.
[28] S. Watcharotone, D.A. Dikin, S. Stankovich, R. Piner, I. Jung, G.H.B. Dommett, et al., Graphene−silica composite thin films as transparent conductors, Nano Letters 7 (7) (2007) 1888–1892.
[29] A. Buchsteiner, A. Lerf, J. Pieper, Water dynamics in graphite oxide investigated with neutron scattering, J Phys Chem B 110 (45) (2006) 22328–22338.
[30] D. Pan, S. Wang, B. Zhao, M. Wu, H. Zhang, Y. Wang, et al., Li storage properties of disordered graphene nanosheets, Chem Mater 21 (14) (2009) 3136–3142.
[31] P. Lian, X. Zhu, S. Liang, Z. Li, W. Yang, H. Wang, Large reversible capacity of high quality graphene sheets as an anode material for lithium-ion batteries, Electrochim Acta 55 (12) (2010) 3909–3914.
[32] A. Chavez-Valdez, M.S.P. Shaffer, A.R. Boccaccini, Applications of graphene electrophoretic deposition. A review, J Phys Chem B 117 (6) (2012) 1502–1515.
[33] Tripathi M, Mahmood H, Novel D, Iacob E, Vanzetti L, Bartali R, et al. Nanoscale friction of graphene oxide over glass-fibre and polystyrene Composites Part B: Engineering (submitted for publication).
[34] S. Pei, H.-M. Cheng, The reduction of graphene oxide, Carbon 50 (9) (2012) 3210–3228.
[35] A. Dorigato, A. Pegoretti, Tensile creep behaviour of polymethylpentene–silica nanocomposites, Polym Int 59 (6) (2010) 719–724.
[36] Rao S, Upadhyay J, Das R. 8 - Manufacturing and characterization of multifunctional polymer-reduced graphene oxide nanocomposites A2 - Dong, Yu. In: Umer R, Lau AK-T, editors. Fillers and Reinforcements for Advanced Nanocomposites: Woodhead Publishing; 2015. p. 157–232.
[37] L. Chen, H. Jin, Z. Xu, M. Shan, X. Tian, C. Yang, et al., A design of gradient interphase reinforced by silanized graphene oxide and its effect on carbon fiber/epoxy interface, Mater Chem Phys 145 (1–2) (2014) 186–196.
[38] W. Qin, F. Vautard, L.T. Drzal, J. Yu, Mechanical and electrical properties of carbon fiber composites with incorporation of graphene nanoplatelets at the fiber–matrix interphase, Compos B Eng 69 (2015) 335–341.
[39] R.L. Zhang, B. Gao, W.T. Du, J. Zhang, H.Z. Cui, L. Liu, et al., Enhanced mechanical properties of multiscale carbon fiber/epoxy composites by fiber surface treatment with graphene oxide/polyhedral oligomeric silsesquioxane, Compos A Appl Sci Manuf 84 (2016) 455–463.
[40] C. Deng, J. Jiang, F. Liu, L. Fang, J. Wang, D. Li, et al., Effects of electrophoretically deposited graphene oxide coatings on interfacial properties of carbon fiber composite, J Mater Sci 50 (17) (2015) 5886–5892.
[41] X. Zhang, X. Fan, C. Yan, H. Li, Y. Zhu, X. Li, et al., Interfacial microstructure and properties of carbon fiber composites modified with graphene oxide, ACS Appl Mater Interfaces 4 (3) (2012) 1543–1552.